南京航空航天大学

论文集

（二〇〇〇年）

第9册

三院

南京航空航天大学科技部编

二〇〇一年六月

三　　院

〇三一系

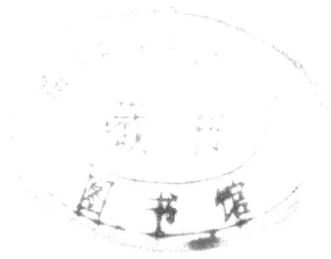

目 录

序号	姓名	职称	单位	论文题目	刊物、会议名称	年、卷、期	类别
261	江　驹 吴树范 龚华军	讲师	031	再入大气层航天飞机的动力学建模与仿真	南京航空航天大学学报	003206	J
262	胡小兵 江　驹	硕士	031	TSP 的一种改进遗传算法	中南工业大学学报	0031 专	H
263	杨一栋 龚华军	教授	031	光传系统地面半物理仿真验证	航空兵器	000001	
264	杨一栋 杨　京 段朝阳	教授	031	大迎角机动导弹飞控系统设计研究	战术导弹控制技术	000002	
265	杨　京 杨一栋 范彦铭	博士	031	基于模糊逻辑的飞行/推力综合控制系统研究	南京航空航天大学学报	003201	J
266	杨　莉 袁　信	讲师	031	基于模糊神经网络的惯性导航系统预热控制	中国惯性技术学报	000803	J
267	范胜林 段志勇 袁　信 胡国辉	讲师	031	非线性滤波及其在 GPS 航姿系统中的应用	数据采集与处理	001503	H
268	范胜林 孙永荣 袁　信	讲师	031	捷联系统陀螺静态漂移参数和标定	中国惯性技术学报	000801	J
269	范胜林 胡国辉 袁　信	讲师	031	低成本 GPS 姿态测量系统	导航	000001	
270	范胜林 袁　信	讲师	031	机动弹头姿态解耦控制方法研究	南京航空航天大学学报	003205	J
271	张乃镇 刘建业 何秀凤	硕士	031	Windows 操作系统下 GPS 接收程序设计	全球定位系统	002503	
272	刘建业 徐　珍 杨　莉 肖纪立	教授	031	Inertial Integrated System of North-Seeking/Sight-Stabilizing on Vehicle	南京航空航天大学学报（英文版）	001702	J
273	徐　珍 杨　莉 刘建业	硕士	031	车载惯性稳瞄/寻北组合系统研究	测控技术	001905	J
274	张乃镇 汤　峰 刘建业	硕士	031	Visual C^{++}开发的导弹伺服机构测控系统	计算机自动测量与控制	000803	J
275	胡小兵 江　驹	硕士	031	TSP 的一种改进遗传算法	中南工业大学学报	0031 专	H
276	孙永荣 刘建业 陆　涛	讲师	031	基于自适应滤波的车载 DR 系统研究	南京航空航天大学学报	003204	J
277	杨　莉 徐　珍 袁　信 刘建业	讲师	031	单动调式陀螺寻北系统及其转位方案	南京航空航天大学学报	003205	J

QFT-Based Robust/Fault-Tolerant Flight Control Design for a Remote Pilotless Vehicle

Shu-Fan Wu, Michael J. Grimble, and Wei Wei

Abstract—**Quantitative feedback theory (QFT) was applied successfully to enhance the robust stability and tracking performance of the pitch flight control system for a remote pilotless vehicle (RPV), within its full flight envelope. The influence of control surface loss or damage to the dynamic derivatives of the aircraft model can be treated as an extension of the model uncertainty robustness problem. QFT is applied to the analysis and design of the fault tolerant flight control system allowing for possible control surface damages.**

Index Terms—**Fault tolerance, flight control, quantitative feedback theory (QFT), robustness.**

I. Introduction

RECENT control design research has concentrated on the development of control systems that are robust to plant variations and parametric uncertainties. These robust control techniques are particularly useful for the design of aircraft flight control systems (FCSs), partly because aircraft dynamics vary substantially throughout the flight envelope. Variables such as airspeed, flight altitude, fuel consumption, and the amount and location of payload, can have a dramatic effect on the aircraft's model parameters and even on the model structures.

One approach to designing robust control systems is through the use of quantitative feedback theory (QFT), which was developed by Horowitz [1] in the early 1970s and has attracted considerable interest over the last two decades [9], [10]. QFT is a frequency domain-based design technique where the controllers can be designed to achieve a set of performance and stability objectives over a specific range of plant parameter uncertainty. The QFT approach (unlike H_∞ and LQG control) is based on classical ideas of frequency domain shaping of the open-loop transfer function. It also differs in the way that uncertainties are characterized [6].

In the last ten years, the application of QFT in FCS design has been studied extensively [2]–[6]. Much of this flight control research was supported by the Air Force Research Laboratory of Wright-Patterson Air Force Base, Dayton, OH [2]–[5], which has culminated in the design and first successful flight testing of a QFT FCS.

This paper is organized in six sections. Section II outlines the QFT design method. Section III describes the original pitch FCS of the RPV considered. Section IV describes the robust FCS design process. Section V discusses the fault-tolerant FCS when the elevator surface damage is considered. The conclusions are summarized in the last section.

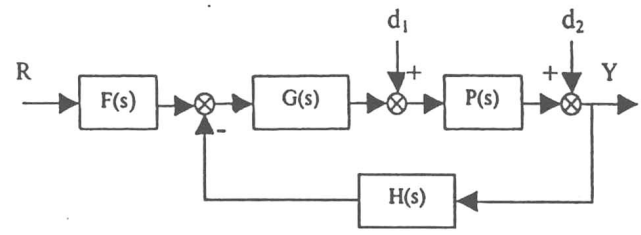

Fig. 1. A canonic two degree-of-freedom feedback structure.

II. Quantitative Feedback Theory

QFT is a robust control design technique that uses feedback of measurable plant outputs to generate an acceptable response from a system in the face of disturbance signals and structured plant modeling uncertainty. Specifically, it employs a two degrees-of-freedom control structure which uses output feedback, a cascade compensator $G(s)$, and a prefilter $F(s)$ to reduce the variations of the plant output due to plant parameter variations and disturbances, as shown in Fig. 1. A fixed sensor dynamics, $H(s)$, in the feedback loop is considered here for more general cases. The QFT method takes into account *quantitative* information on the plant's variability, the robust performance requirements, tracking performance specifications, the expected disturbance amplitude and its attenuation requirements. The compensator is designed to ensure that robustness and disturbance rejection requirements can be met. The prefilter is then used to tailor the step response to meet the control specifications.

The QFT designs are undertaken with the *Nichols chart*, a plot of phase as abscissa and log magnitude as ordinate, both parameterized by frequency. Because a whole set of plants, rather than a single plant is considered, the magnitude and phase of the plants (at each selected frequency) yields a set of points on the Nichols chart, instead of a single point, which form a connected region, or so-called *template*. Larger templates indicate greater uncertainty. These templates are then used to define regions (or so-called *bounds*) in the frequency domain where the system open-loop frequency response must lie. The *stability bounds* are calculated using these templates and the phase margin. The *performance bounds* are derived using the templates and the upper and lower limits on the frequency-domain responses. The upper limit of the *disturbance bounds* is derived based on the disturbance rejection specifications.

Manuscript received September 28, 1998; revised October 7, 1999. Recommended by Associate Editor, S. Banda.

S.-F. Wu and W. Wei are with the Department of Automatic Control, Nanjing University of Aeronautics and Astronautics, Nanjing 210016, China (e-mail: zenac@nuaa.edu.cn).

M. J. Grimble is with the Industrial Control Centre, University of Strathclyde, Glasgow G1 1QE, U.K. (e-mail: m.grimble@eee.strath.ac.uk).

Publisher Item Identifier S 1063-6536(00)07358-9.

TABLE I
FLIGHT CONDITIONS CONSIDERED IN THE FULL FLIGHT ENVELOPE

Flight Cond.	1	2	3	4	5	6	7	8
Speed (m/s)	86.31	229.61	220.58	139.62	137.28	207.61	90.61	74.07
Altitude(m)	1.51	3564	5069	975.3	493	602	1440	360
Weight(kg)	2359.4	2313.85	2268.52	2222.97	2218.93	2142.79	1548.87	1527.54

The compensator is determined through the *loop shaping* process, using a Nichols chart that displays the stability, performance, and disturbance rejection bounds. The disturbance rejection and tracking action of the compensator is based on keeping the loop transfer gain above the disturbance and tracking performance bounds on the Nichols chart. The stability performance is achieved by keeping the loop transfer function outside the corresponding stability bounds at appropriate frequencies [6]. During the loop shaping process, modifying the poles and zeros of the compensator produces immediately visible results, enabling the designer to examine the tradeoffs between compensator complexity and system performance [7]. Finally, the prefilter design is conducted using a Bode diagram to shape the closed-loop frequency response, so as to satisfy the tracking performance requirement. A detailed description about the principle and design procedure is recommended to the reference [6].

QFT was devised to design robust controllers for highly uncertain, linear time invariant (LTI), single-input/single-output (SISO) systems. Recent research has extended the technique to handle multiinput/multioutput (MIMO) [9], nonlinear and time varying plants [10]. MIMO systems are mathematically decomposed into their multiinput/single-output (MISO) counterparts, where the coupling between the channels is treated as a disturbance that needs to be rejected. A beneficial byproduct of MIMO QFT design is the approximate decoupling of the resulted closed-loop robust control system.

III. PITCH FLIGHT CONTROL SYSTEM

The CK-I series of unmanned aircraft was developed in the early 1980s by Nanjing University of Aeronautics and Astronautics (NUAA) for multiple applications, and has been put into many practical and special applications successfully in the past two decades. The pitch attitude FCS redesign with QFT is considered in the following. The simplified short-period dynamic model, linearized with small perturbations, has following form [8]:

$$\begin{cases} (D + n_{22})\Delta\alpha - (D + n_{23})\Delta\theta = -n_{24}\Delta\delta_e \\ (n_{00}D + n_{32})\Delta\alpha + (D^2 + n_{33}D)\Delta\theta = -n_{34}\Delta\delta_e \end{cases} \quad (1)$$

where

θ	pitch attitude angle;
α	attack angle;
$\Delta\delta_e$	elevator deflection angle;
n_{xx}	dynamic derivatives;
D	differential operator.

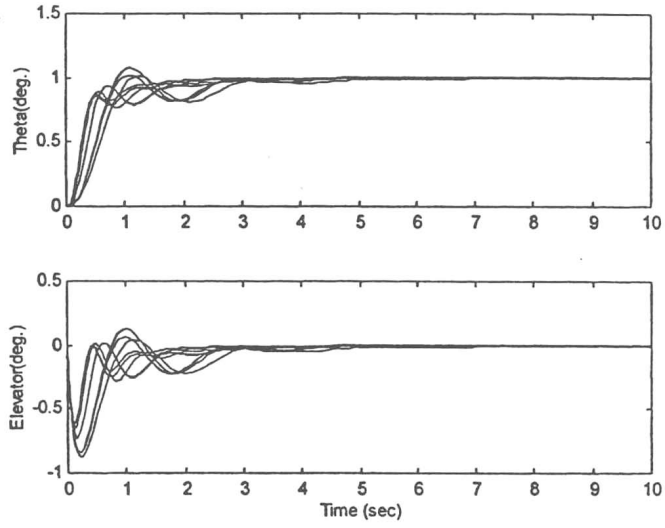

Fig. 2. Aircraft pitch angle unit step responses.

For this aircraft model, the existing pitch attitude control law was given as [8]

$$(T_e s + 1)\Delta\delta_e = K_\theta(\Delta\theta - \Delta\theta_c) + K_{\dot\theta}\Delta\dot\theta \quad (2)$$

where

$\Delta\theta_c$	input pitch angle command signal;
$T_e = 0.1$ s	time constant of the elevator actuator dynamics;
$K_\theta = 1.1$ and $K_{\dot\theta} = 0.2$	control gains.

To check the control performance over its full flight envelope, eight typical flight conditions are considered, as illustrated in Table I. The simulated time responses of the aircraft to a step pitch angle command at the eight flight conditions are illustrated in Fig. 2. As shown, the performance at different flight conditions varies a lot. At some conditions, large overshoots and oscillations appear. Also, the stability margins were not considered during the design, with the consequence that they are found to be very small, about 1.2 dB in gain and 10° in phase.

IV. ROBUST FLIGHT CONTROLLER DESIGN

A. Problem Formulation

To enhance the performance and stability robustness of the pitch FCS, the QFT approach is used here to modify (or redesign) the control law. The pitch FCS is first formulated as a single loop SISO system, as illustrated in Fig. 1. The input

signal is the pitch attitude angle command, the output is the actual pitch attitude angle of the aircraft, and the transfer function of the plant (with uncertainty) is described by the following equation, as derived from (1):

$$P(s) = \frac{-1}{T_e s + 1} \frac{\Delta\theta(s)}{\Delta\delta_e(s)} = \frac{-1}{T_e s + 1} \frac{as + b}{s^3 + cs^2 + ds + e} \quad (3)$$

where

$$\begin{aligned} a &= n_{00}n_{24} - n_{34}; \\ b &= n_{24}n_{32} - n_{22}n_{34}; \\ c &= n_{00} + n_{22} + n_{33}; \\ d &= n_{22}n_{33} + n_{00}n_{23} + n_{32}; \\ e &= n_{23}n_{32}. \end{aligned}$$

The sensor dynamics in the feedback loop, representing both the pitch angle and the pitch rate feedback, is expressed by

$$H(s) = (K_{\dot\theta}s + K_\theta)/K_\theta = \tau_\theta s + 1 \quad (4)$$

where $\tau_\theta = K_{\dot\theta}/K_\theta = 0.182$, taking the value from the original control gains.

B. Performance Specifications

The *tracking specification* defines the acceptable range of variations in the closed loop tracking responses of the system due to uncertainty and disturbances. It is generally defined in the time-domain, but normally transformed into the frequency domain, as expressed by the following:

$$T_{RL}(j\omega) \le T_R(j\omega) \le T_{RU}(j\omega) \quad (5)$$

where the function $T_R(s)$ denotes the closed-loop transfer function and $T_{RL}(s)$ and $T_{RU}(s)$ the equivalent transfer functions of the lower and upper tracking bounds. For the pitch FCS, an overshoot of less than 2% and a settling time of less than 3 s are specified, and the equivalent bound transfer functions can be constructed as follows:

$$\begin{aligned} T_{RL}(s) &= \frac{48}{(s+1.5)(s+4)(s+8)} \\ T_{RU}(s) &= \frac{6.25(0.2s+1)}{s^2 + 3.9s + 6.25}. \end{aligned} \quad (6)$$

For robust stability margins, the gain margin is expected to be greater than 3.5 dB and the phase margin angle to be larger than 30°. Thus the robust stability specification is defined as

$$\left| \frac{P(j\omega)G(j\omega)H(j\omega)}{1 + P(j\omega)G(j\omega)H(j\omega)} \right| \le M_m = 1.8 \quad (7)$$

which corresponds to a lower gain margins of $K_M = 1 + 1/M_m = 1.556 = 3.84$ dB and a phase margin angle of $\gamma = 180 - \cos^{-1}(0.5/M_m^2 - 1) = 32°$.

No *disturbance rejection specifications* are given here, partly since the disturbance rejection requirements can often be treated as a byproduct of satisfying the tracking specifications.

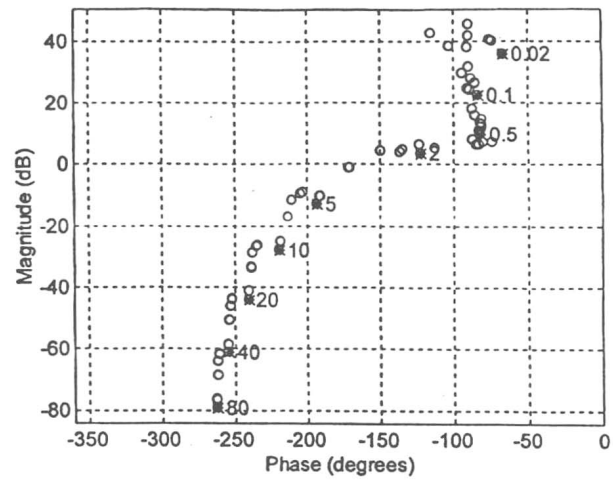

Fig. 3. Plant frequency response templates.

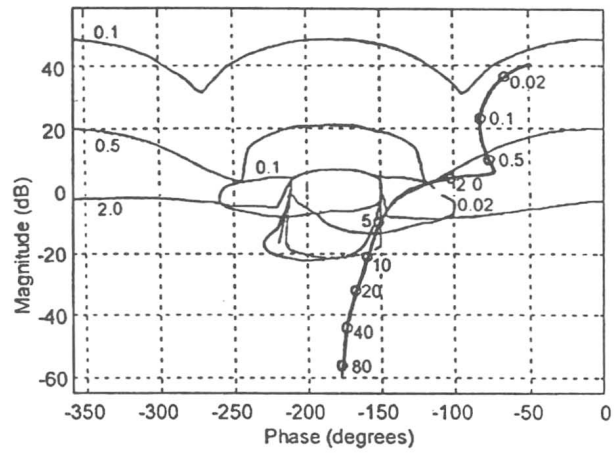

Fig. 4. Open-loop frequency response without controller.

C. Robust Controller Design with QFT

A trial frequency array, a set of separate points in the frequency spectrum, should be determined based on the plant dynamics and the specifications, so that all of the frequencies that are important to the design are represented in the templates and boundaries. Initially it was chosen as $\omega = \{0.02, 0.1, 0.5, 5, 20, 80\}$, but computation results showed that the frequency range between 0.5\–20 had great influences on the stability margins. Thus more points in this range were added to the array, which was finally chosen as $\omega = \{0.02, 0.1, 0.5, 2, 5, 10, 20, 40, 80\}$. Second, a nominal plant should be chosen for the loop shaping. Based on the analyzes of the frequency bandwidth and template boundary shapes, the flight condition 8 was chosen as the nominal plant.

Using the Matlab QFT Toolbox [7], the plant templates at the frequency array are computed, as illustrated in Fig. 3, where the nominal plant is indicated by a star in the templates. The performance bounds are then computed based on the performance specifications and the plant templates, as depicted in Fig. 4. The closed round lines in the central area represent the robust stability bounds, the wavy lines in the upper area represent the tracking performance bounds at different trial frequencies, and the vertical curve line represents the frequency response

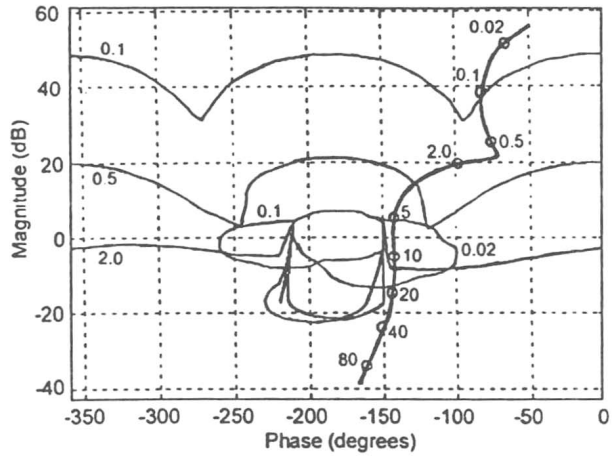

Fig. 5. Open-loop frequency response with controller.

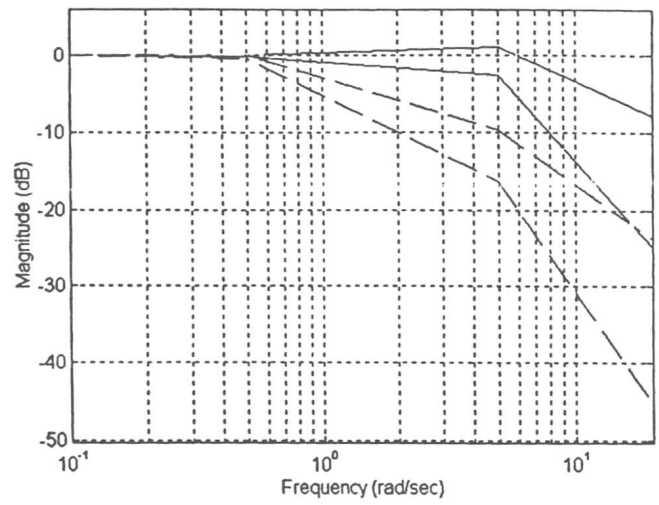

Fig. 6. Closed-loop frequency response without prefilter.

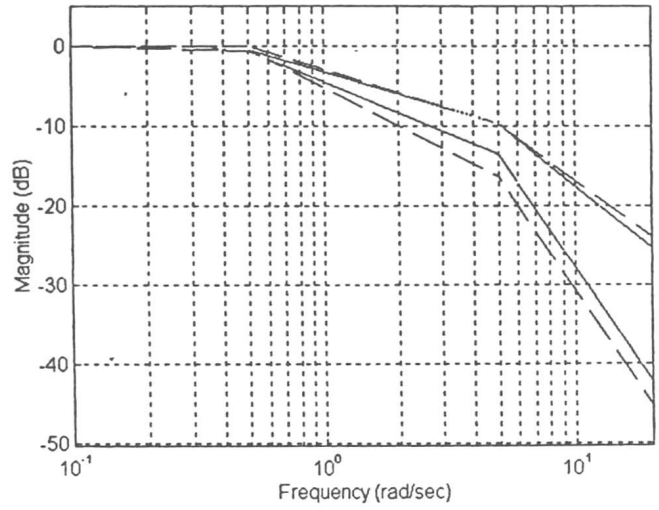

Fig. 7. Closed-loop frequency response with prefilter.

of the nominal open-loop transfer function with the controller $G(s) = 1$.

The controller design then proceeds using the Nichols chart and classical loop-shaping ideas. The objective is to synthesize a controller, $G(s)$, which satisfies the design specifications whilst minimizing the controller bandwidth. Fig. 4 also shows the frequency response of the nominal open-loop transfer function, which violates the stability bounds. The design objective is to apply dynamic compensation to the nominal open-loop transfer function, so that the performance bounds are satisfied at each frequency. From Fig. 4, the open-loop frequency response is located below the appropriate tracking performance bounds at each trial frequency. Thus an appropriate control gain should be introduced to push the open-loop frequency response upwards. Moreover, the open-loop frequency response has also crossed the stability bounds. Hence a dynamic compensator is required to change the shape of the open-loop frequency response. Analysis and trial show a lead compensator with a 23.84 degree of phase lead at the frequency of 26.85 should be introduced. The controller was finally designed as

$$G(s) = \frac{5.7(s/17.5+1)}{s/41.2+1} = \frac{5.7(2.35s+41.2)}{s+41.2}. \quad (8)$$

The resultant open-loop frequency response with this controller is illustrated in Fig. 5. As can be seen, the resultant open-loop frequency response still goes through an stability bound. Analyzes show this stability bound corresponds to the trial frequency of 0.02 rad/s, but the segment of the open-loop frequency response within this stability bound correspond to a frequency range of 5–20 rad/s. Thus the open-loop frequency response actually does not violate the stability performance requirements. The stability performance analysis of the closed-loop system in the next section also supports this point, as shown in Fig. 12.

The controller design has reduced the variations in the closed-loop frequency response to the desired range. A prefilter is then designed to achieve the required shape of the closed-loop frequency response. Fig. 6 shows the Bode magnitude plot of the closed-loop frequency response without a prefilter, together with the tracking frequency response specifications plotted with dashed lines. Obviously a dynamic prefilter is required to shape the frequency response to be within the desired range. It was finally designed as

$$F(s) = \frac{s/12+1}{s/1.4+1} = \frac{0.12s+1.4}{s+1.4}. \quad (9)$$

The resulting closed-loop frequency response with this prefilter is illustrated in Fig. 7.

D. Performance Validation and Simulation

The robust pitch flight controller was finally obtained as

$$\begin{aligned}(T_e s+1)\Delta\delta_e(s) &= -G(s)[F(s)\theta_c - H(s)\theta] \\ &= \frac{s/17.5+1}{s/41.2+1}\left(5.7\theta + \dot{\theta} - \frac{5.7s/12+5.7}{s/1.4+1}\theta_c\right). \quad (10)\end{aligned}$$

Analyzes of the closed-loop system performance in the frequency domain show that the worst closed-loop response

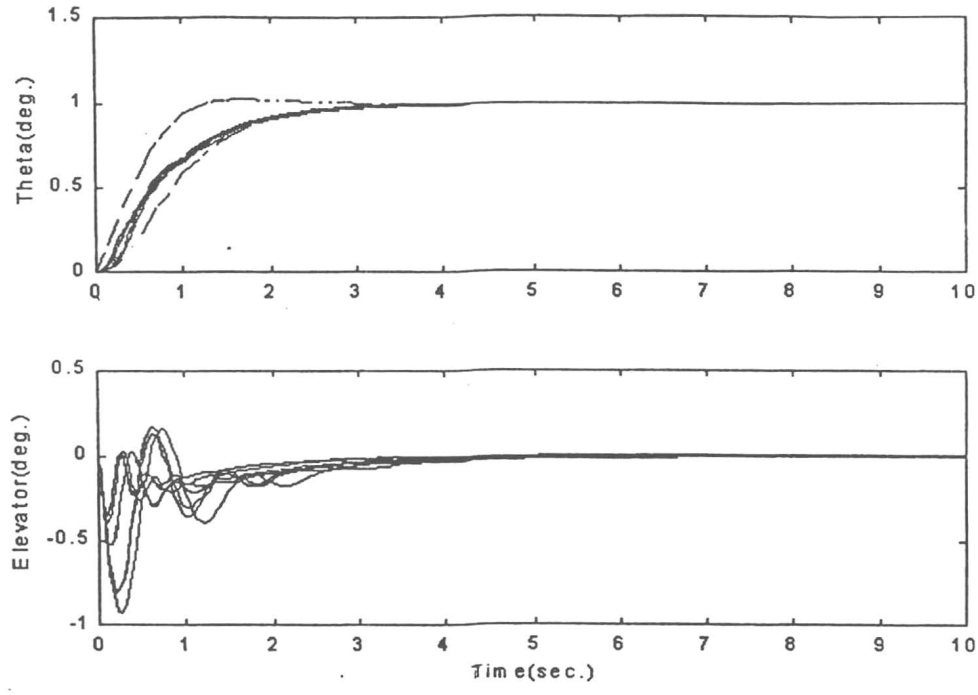

Fig. 8. Step responses of the deigned robust FCS.

magnitude (covering all uncertainty cases) is well below the specified value [refer to (7)], as illustrated in Fig. 12. The maximum variation of the closed-loop system frequency response is well within the specified range [refer to (6)], as illustrated in Fig. 13. Thus the closed-loop control system has met all the design specifications in the full flight envelope. The time-domain simulation results, illustrated in Fig. 8 together with the specified tracking bounds plotted with dashed lines, further support the above conclusion.

V. Robust/Fault–Tolerant Controller Design

When damage to control surfaces occurs, an aircraft partially loses the ability to generate moments about its axes. The aircraft then experiences a change in its dynamic responses, because loss of an aerodynamic surface changes the stability derivatives of the aircraft. Up to 50% of the elevator surface loss is considered here, which is modeled as the decreases in the corresponding control derivatives. Specifically the control derivatives n_{24} and n_{34} in equation (1) are changed by multiplying a factor from 0.5 to 1.0 with step 0.1, and the effects on other dynamic derivatives of the aircraft are neglected. Thus each flight condition yields six different model parameters. From an uncertainty viewpoint, the uncertainty range has been increased to 48 structured plant models in the full envelope. The time responses of the original controller, (2), under the 48 flight conditions are depicted in Fig. 9, which reveals even larger and worse variations in the performance.

Using the same performance specifications, given in Section IV-B, QFT designs were conducted for this larger plant uncertainty. A lead compensator was used with 29.75 degree of phase lead at the frequency of 23 rad/s, together with an even

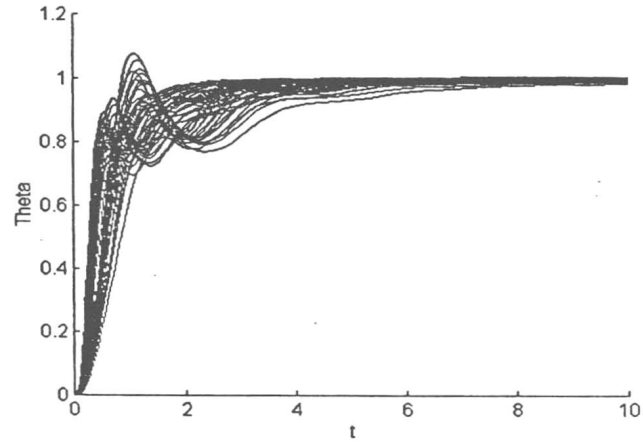

Fig. 9. Step responses of the original FCS at 48 different states.

higher control gain. The resultant compensator and prefilter were obtained as

$$G(s) = \frac{11.5(s/13.4+1)}{s/40+1} = \frac{11.5(2.99s+40)}{s+40},$$
$$F(s) = \frac{s/8.3+1}{s/1.3+1} = \frac{0.156s+1.3}{s+1.3} \tag{11}$$

The resultant time-domain simulation results are illustrated in Fig. 10. Due to the higher plant uncertainty, a higher control gain, 11.5 must be used. This can be difficult for engineering implementation, and also lead to high elevator deflections, or even to elevator saturation, which are not expected practically. For the unit step input, as shown in Fig. 10, the maximum elevator deflection had reached 1.9°, much higher than its original value, around 0.8 as shown in Fig. 2.

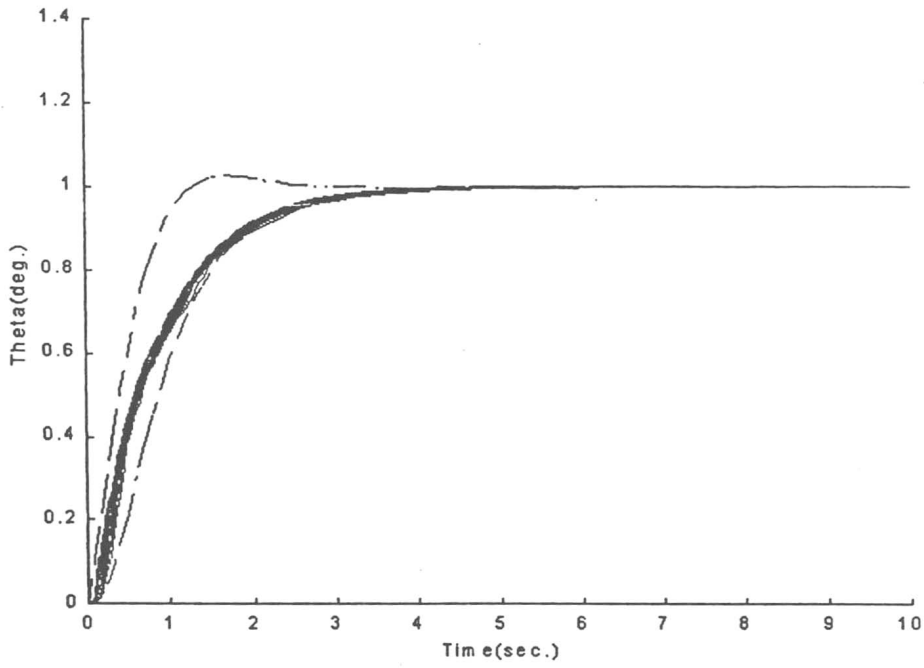

Fig. 10. Step responses of the FCS with controller of (11).

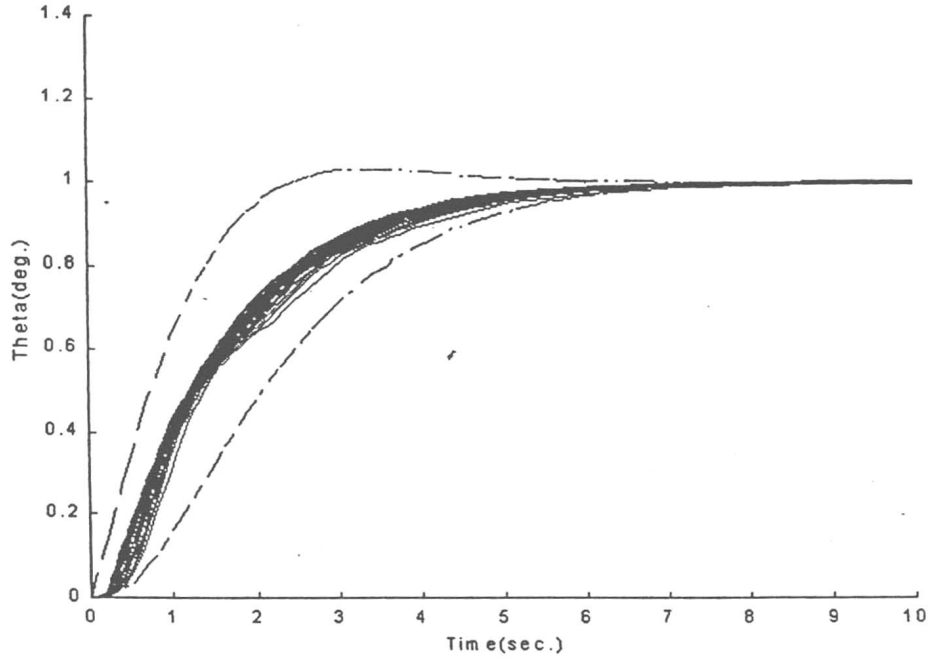

Fig. 11. Step responses of the FCS with controller of (13).

In principle, the damaged loss in elevator will ease the aircraft performance, e.g., longer setting time, and etc. To reduce the control gain and to show the feasibility of QFT in fast redesign and in the tradeoffs between the performance specifications and the controller complexity, a new slower tracking performance specification was applied, in which the settling time requirement was changed to be less than 5 s. The bound transfer-functions then became

$$T_{RL}(s) = \frac{4}{(s+0.8)(s+1)(s+5)},$$

$$T_{RU}(s) = \frac{0.72s + 1.44}{s^2 + 1.872s + 1.44} \tag{12}$$

And the QFT design results became

$$G(s) = \frac{3.2(s/7.5+1)}{s/14.3+1} = \frac{3.2(1.9s+14.3)}{s+14.3},$$
$$F(s) = \frac{0.75}{s+0.75}. \tag{13}$$

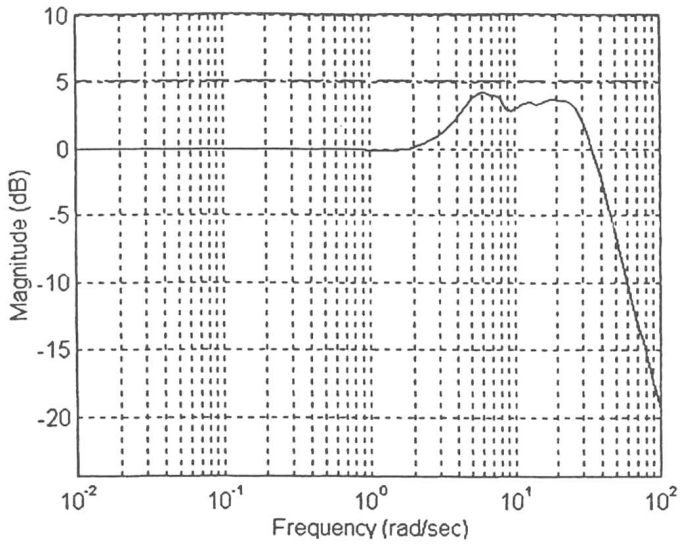

Fig. 12. Analysis of the closed-loop robust stability margins.

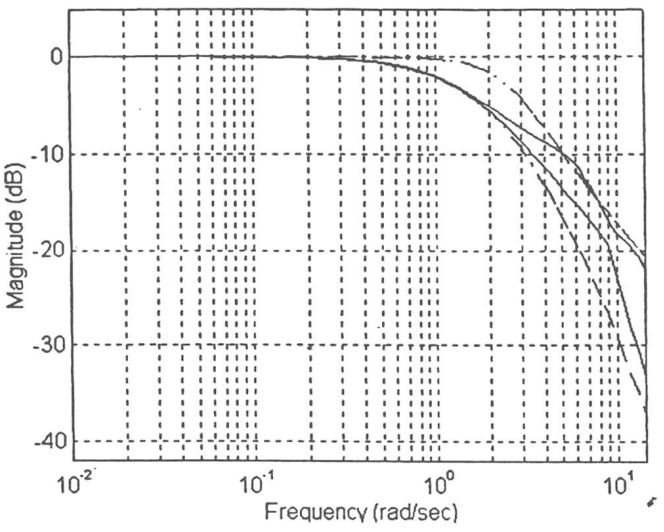

Fig. 13. Analysis of the closed-loop tracking frequency responses.

The appropriate time domain simulation results are shown in Fig. 11, where the maximum elevator deflection is reduced to 0.58°, which is even smaller than the value with the original controller. Thus it is more feasible for practical implementations.

VI. Conclusion

The QFT approach can be used to enhance the robust stability and tracking performance of the existing FCS. A single robust controller and prefilter was designed for the pitch attitude angle control system, which met the frequency domain tracking specifications and robust stability requirements throughout the full flight envelope.

The aircraft control surface loss can be modeled as a kind of parameter uncertainty, or a kind of structured plant uncertainty. Hence, the QFT approach can further be used to the fault-tolerant FCS design.

The redesign and tradeoffs between the system performance specifications and the controller complexity can easily be done, which provides the designer with more versatile solutions. The QFT synthesized FCS is an effective control system, that does not require the use of gain scheduling, and involves a simple low-order fixed controller.

References

[1] I. M. Horowitz and M. Sidi, "Synthesis of feedback systems with large plant ignorance for prescribed time domain tolerance," *Int. J. Contr.*, vol. 16, no. 2, pp. 287–309, 1972.

[2] M. S. Keating, M. Pachter, and C. H. Houpis, "QFT applied to fault tolerant flight control system design," in *ACC Proc.*, June 1998, pp. 184–188.

[3] O. R. Reynolds, M. Pachter, and C. H. Houpis, "Full envelope flight control system design using quantitative feedback theory," *J. Guidance, Contr., Dyn.*, vol. 19, no. 1, pp. 23–29, 1996.

[4] S. A. Snell and P. W. Stout, "Quantitative feedback theory with a scheduled gain for full envelope longitudinal control," *J. Guidance, Contr. Dyn.*, vol. 19, no. 5, pp. 1095–1101, 1996.

[5] P. L. Fontenrose and C. E. Hall, "Development and flight testing of quantitative feedback theory pitch rate stability augmentation system," *J. Guidance, Contr., Dyn.*, vol. 19, no. 5, pp. 1109–1115, 1996.

[6] S.-F. Wu, M. J. Grimble, and S. G. Breslin, "Introduction to quantitative feedback theory for lateral robust flight control system design," *IFAC J. Contr. Eng. Practice*, vol. 6, no. 7, pp. 805–827, 1998.

[7] C. Borghesani, Y. Chait, and O. Yaniv, *Quantitative Feedback Theory Toolbox: For Use with Matlab (User's Guide)*. Natick, MA: The Math Works, Inc., Dec. 1994.

[8] "Dynamic physical simulation test of the KJ-9 autopilot," NUAA, Tech. Rep., Aug. 1981.

[9] C. H. Houpis, "Quantitative feedback theory (QFT): Techniques for designing multivariable control systems," Wright-Patterson Air Force Base, OH, AFWAL-TR-86-3107, 1987.

[10] I. M. Horowitz, *Quantitative Feedback Design Theory*. Boulder, CO: QFT, 1993, vol. 1.

第21卷 第4期
2000年10月

宇 航 学 报
JOURNAL OF ASTRONAUTICS

Vol.21 No.4
Oct. 2000

GPS定位定向系统的研究

胡国辉 范胜林 袁 信

(南京航空航天大学自控系·南京·210016)

摘 要 本文提出一种综合模糊度搜索算法和余度测量的周跳检测法。采用该方法进行模糊度搜索，保证了初始化时间最短的组合能在300秒以内出现，使初始化时间大大缩短。

主题词 载波相位 整周模糊度 Cholesky分解 姿态测量 Kalman滤波

RESEARCH OF GPS POSITIONING AND HEADING SYSTEM

Hu Guohui Fan Shenlin Yuan Xin

(Department of Automatic Control of Nanjing University of Aeronautics & Astronautics·Nanjing·210016)

Abstract The paper present a kind of ambiguity search algorithm and a kind of cycle slip detection algorithm with redundant measurements. The test results show that the method can ensure the combination of the shortest intial time will appear within 300 seconds and the initial time can reduce rapidly.

Key words Carrier phase Ambiguity Cholesky facetorization Attitude determination Kalman filtering

1 引言

采用载波相位差分测量姿态，需要解决快速、准确、可靠地确定模糊度的问题。载波相位差分用于静态定位则是确定相对地球坐标系静止不动的用户接收天线与基准站之间的相对位置，其相对基准站的位置和模糊度可以通过多个历元、多个时刻的观测数据求解，求解方法相对简单。在动态定位中，由于载波相位观测值在不发生周跳的情况下，其模糊度数值不变，因而可以利用静态定位的方法首先进行静态观测，待模型度正确求解之后再进行动态测量，或者占据一条已知基线，利用已知的基线向量来反求模糊度。静态定位方法应用于动态定位中，原理简单，软件实现方便，在早期的载波相位动态定位软件中得到了广泛的应用。但这种方法均需在动态定位开始之前进行，并在动态定位中连续跟踪4颗以上卫星，而一旦因周跳或失锁使连续跟踪的卫星少于4颗，则高精度的动态定位无法继续，限制了载波相位在GPS动态定位和姿态测量中的应用。因而国内外GPS专家开始寻

收稿日期：1999年7月21日，修回日期：2000年3月15日

*国防预言基金资助项目

找能在运动中求解模糊度的方法，即整周模糊度的在航解算（Ambiguity Resolution On the Fly 或者 On the Fly），称为 AROF 或 OTF。

OTF 近年来已成为国内外 GPS 专家研究的热点问题。总的说来可分为四类，双频伪距法，模糊函数法，最小二乘法和模糊度协方差法。其中最为著名的有优化 Cholesky 分解算法[1]，快速模糊度滤波法，LAMBDA 法，整数非线性规划法和基因法。

以上各种模糊度的搜索算法均有其优缺点，优化 Cholesky 分解算法能有效地利用以前的信息，但由于换星（主星变化、可见星变化），纬数不确定，采用所有可见星的 Cholesky 分解算法编程复杂，且搜索范围较大，难以满足实时性。最小二乘法[2]将卫星分为两组，选4颗主星作为基本搜索组，其余卫星作为检验组。但这种方法搜索量较大，且不能有效采用 Kalman 滤波器利用以前信息。结合两种方法，我们探索出“综合模糊度搜索算法”，采用 Kalman 滤波器将模糊度作为状态估计，选5颗主星进行 Cholesky 分解，利用其余卫星进行检验。

周跳检测和修复是载波相位动态定位中的另一关键问题。由于载波相位测量只能测量相位中不足一整周的小数部分，连续整周部分由多普勒记数得到，信号的遮挡、信噪比低以及接收机故障都可引起整周记数的突变一周跳。如果利用 OTF 技术能在一个历元之内确定整周模糊度，则对周跳的检测、修复的研究可不必继续下去。由于卫星数、卫星图形、观测条件等的不同，在一个历元内实现 OTF 解算模糊度还存在困难，因而对周跳的检测和修复进行研究仍具有重要意义。

动态环境中周跳的检测和修复与静态测量相比较更为困难。动态定位中由于运载体在不断运动中，且相对每一动态方位观测值较少，在静态定位中十分有效的高次差法、双差法等均难以适用。Wei[3]利用 Kalman 滤波新息序列来进行周跳探测，然而探测周跳的能力与载体的动态变化有关，动态变化越剧烈探测能力越低。

以上周跳检测和修复方法，受载体的动态影响大。在研制样机时我们除了在静态采用多式拟合法进行周跳检测外，还探索出在动静态都能运用的“余度测量的故障检测法”。

2 综合模糊度搜索算法

为了充分利用以前的测量信息，仍然利用 Kalman 滤波器求取模糊度的浮点解[1]，对于双天线 GPS 载波相位测量，系统的状态方程和观测方程为：

$$\begin{cases} X_k = AX_{k-1} + \xi_{k-1} \\ y_k = HX_k + \eta_k \end{cases} \tag{1}$$

其中：

$$X_k^T = [x\ y\ z\ \dot{x}\ \dot{y}\ \dot{z}\ N_1\ N_2 \cdots\ N_n]$$

$$y_k^T = [\varphi_1\ \varphi_2 \cdots\ \varphi_n]$$

$$A = \begin{bmatrix} I_{3\times3} & 0_{3\times3} & 0_{3\times n} \\ \Delta T I_{3\times3} & I_{3\times3} & 0_{3\times n} \\ 0_{n\times3} & 0_{n\times3} & I_{n\times n} \end{bmatrix}$$

$I_{i\times j}$、$0_{i\times j}$分别为$i\times j$单位矩阵、零矩阵。

$$H=\begin{bmatrix} e_{11} & e_{12} & e_{13} & 0_{1\times 3} & -\lambda & & \\ e_{21} & e_{22} & e_{23} & 0_{1\times 3} & & -\lambda & \\ \cdots & \cdots & \cdots & & \ddots & & \\ e_{n1} & e_{n2} & e_{n3} & 0_{1\times 3} & & & -\lambda \end{bmatrix}$$

$X_x=[x\ y\ z\ \dot{x}\ \dot{y}\ \dot{z}]$ 为基线向量和基线速度，$X_N=[N_1\ N_2\cdots\ N_n]$ 为双差模糊度，y_k 为载波相位的双差测量值。

$\begin{bmatrix} e_{11} & e_{12} & e_{13} \\ e_{21} & e_{22} & e_{23} \\ \cdots & \cdots & \cdots \\ e_{n1} & e_{n2} & e_{n3} \end{bmatrix}$ 为指向卫星的方向余弦矩阵。

对于式（1）的状态方程和观测方程可以采用卡尔曼滤波器进行估计。

$$\hat{X}_{k+1/k}=\hat{X}_{k/k} \tag{2}$$

$$P_{k+1/k}=AP_{k/k}A^T \tag{3}$$

$$\hat{X}_{k+1/k+1}=\hat{X}_{k+1/k}+K_{k+1}[y_{k+1}-H_{k+1}\hat{X}_{k+1/k}] \tag{4}$$

$$K_{k+1}=P_{k+1/k}H_{k+1}^T[H_{k+1}P_{k+1/k}H_{k+1}^T+R_{k+1}]^{-1} \tag{5}$$

$$P_{k+1/k+1}=(I+K_{k+1}H_{k+1})P_{k+1/k}(I-K_{k+1}H_{k+1})^T+K_{k+1}R_{k+1}K_{k+1} \tag{6}$$

$P0/0$，$X0/0$ 初值的选取取决于对基线向量和初始模糊度范围的了解，如果上述初始范围完全不确定，可取无穷大。当卡尔曼滤波器的滤波达到一定精度后，可进行整周模糊度的搜索。

对于式（6）中的 $P_{k/k}$可以写成：

$$P_k=\begin{bmatrix} P_x & P_{xN} \\ P_{Nx} & P_N \end{bmatrix}$$

P_x、P_N 分别为基线向量与整周模糊度误差的协方差矩阵。

P_{xN}、P_{Nx}分别为它们之间的误差协方差矩阵。

这里选 5 颗主卫星进行 Cholesky 分解，利用其余卫星进行检验。

$$\hat{X}=[\hat{X}_1\quad \hat{X}_2],N=[N_1\quad N_2],P_N=\begin{bmatrix} P_{11} & P_{12} \\ P_{21} & P_{22} \end{bmatrix}$$

N_1、N_2分别为主卫星与其余卫星整周模糊度的整数解，$\hat{X}_1$、$\hat{X}_2$分别为主卫星与其余卫星整周模糊度的浮点解，P_{11}、P_{12}分别为主卫星与其余卫星整周模糊度误差的协方差矩阵，P_{12}、P_{21}分别为它们之间的误差协方差矩阵。

整周模糊度求解应使

$$J = (\hat{X}_1 - N_1)^T P_{11}^{-1} (\hat{X}_1 - N_1) \tag{7}$$

最小，其中N_1为待确定的整周模糊度。

为了使搜索能满足树状规律，可进行下三角分解。

$$P_{11}^{-1} = CC^T \tag{8}$$

其中 $$C = \begin{bmatrix} c_{11} & 0 & 0 & 0 \\ c_{21} & c_{22} & 0 & 0 \\ c_{31} & c_{32} & c_{33} & 0 \\ c_{41} & c_{42} & c_{43} & c_{44} \end{bmatrix}$$

将式（8）带入式（7）可得

$$\begin{aligned} J &= (\hat{X}_1 - N_1)^T P_{11}^{-1} (\hat{X}_1 - N_1) \\ &= (\hat{X}_1 - N_1)^T CC^T (\hat{X}_1 - N_1) \\ &= f^T f = f_1^2 + f_2^2 + f_3^2 + f_4^2 \end{aligned} \tag{9}$$

其中：$f = C^T (\hat{X}_1 - N_1) \triangleq [f_1 \quad f_2 \quad f_3 \quad f_4]$

$\hat{X}_1 = [x_1\ x_2\ x_3\ x_4]$，$N_1 = [n_1\ n_2\ n_3\ n_4]$

$$f_4 = (x_4 - n_4) C_{44} \tag{10a}$$

$$f_3 = (x_4 - n_4) C_{43} + (x_3 - n_3) C_{33} \tag{10b}$$

$$f_2 = (x_4 - n_4) C_{42} + (x_3 - n_3) C_{32} + (x_2 - n_2) C_{22} \tag{10c}$$

$$f_1 = (x_4 - n_4) C_{41} + (x_3 - n_3) C_{31} + (x_2 - n_2) C_{21} + (x_1 - n_1) C_{11} \tag{10d}$$

由于$\hat{X}_1$的误差方差阵为

$$P_{11} = \begin{bmatrix} s_{11} & s_{12} & s_{13} & s_{14} \\ s_{21} & s_{22} & s_{23} & s_{24} \\ s_{31} & s_{32} & s_{33} & s_{34} \\ s_{41} & s_{42} & s_{43} & s_{44} \end{bmatrix}$$

N 的取值范围为 $n_j \in [\text{roung}(x_j - 3\sqrt{s_{jj}}), \text{round}(x_j + 3\sqrt{s_{jj}})](j = 1,\cdots,4)$round 为取整，

如果 $\text{round}(x_j - 3\sqrt{s_{jj}}) = \text{round}(x_j + 3\sqrt{s_{jj}})$

则取 $n_j \in [\text{round}(x_j - 3\sqrt{s_{jj}}) - 1, \text{round}(x_j + 3\sqrt{s_{jj}}) + 1](j = 1,\cdots,4)$

计算量由 $f_4 \to f_1$ 递减，由于 f_i^2 是大于零或等于零，在计算中式(9)和式(10)可以交替计算，当某一检测模糊度 f 部分分量平方和已大于某一限值(可选为前面已经计算的 J 次小值)，则该模糊度组将被拒绝，而不用计算 f 的剩余分量及其平方和，从而大大减少计算量。

最优剪枝法的搜索为一历元的模糊度搜索顺序应从搜索范围的中间向两边进行，这是因为越靠近搜索中心的模糊度组为正确模糊度的可能性越大，其 J 数值一般较搜索空间的边缘要小，从而在上述搜索计算过程中可以进一步减小计算量。搜索过程中只要保留已搜索过的模糊度、模糊度组中 J 为最小及次小的模糊度数值及相应的 J 数值。

对于以上四层树状搜索图仍然采用最优剪枝法进行搜索，满足指标函数最小的解，被认为是整周模糊度的解，但仍需要经过检验，满足求解基线长度与已知基线长度相吻合(实际中二者之差小于 0.02 米即可认为二者相吻合)，即认为通过第一次检验，然后利用前面求出的基线向量对所有载波相位测量求整周模糊度，由于模糊度是整数，因此可以对取整后剩余部分进行残差检验，通过以上两次检验即认为模糊度已固定。采用该方法进行模糊度搜索，保证了初始化时间最短的组合能在 300 秒以内出现，使被始化时间大大缩短；

3　余度测量的周跳检测法

当正确模糊度求解后，如果不发生周跳，则求解的基线向量的基线长度均为已知基线长度（附加测量噪声），当载波相位测量发生周跳后，则求解的基线长度均不与已知基线长度相吻合，这样可以探测到某个载波相位测量发生周跳，但究竟是哪一个载波相位测量发生周跳还需利用余度测量进一步探测，并修复。

在正确模糊度求解后，仅有四颗可见星的载波相位测量就可求出基线向量和基线长度。而一般可见星均在四颗以上。因此可以采用 4 颗星进行组合，如果某四颗星的组合求出的基线长度与已知基线长度吻合，即认为该四颗星的载波相位测量未发生周跳，然后利用这四颗星求出的基线向量可以求出其它的双差模糊度，并与原来的模糊度比较，即可探测出哪个载波相位测量发生周跳，并修复。

4　试验结果及分析

采用两块 *GG24 OEM* 板（*Ashtech*）公司生产）、*PC*104 586 工控机及其接口板构成高精度的 *GPS* 定位定向系统，人机对话方面采用薄膜触摸式键盘，液晶显示，操作简单，仅有几个功能键和 10 个数字键，菜单式显示，可以提供位置、速度、方位角和俯仰角，平均初始化时间小于 180 秒。

其方位角精度通过省计量测试技术研究所的技术标定，测设设备为九江 6354 所生产的精密多齿分度台（分度值 0.5 度，精密 0.2 角秒），试验在南京航空航天大学 15 号楼露天平台上进行，将天线架固定在精密多齿分度台上，精密多齿分度台每隔 30 度，停 1 分

钟，读取 *GPS* 定位定向系统方位角数据，其结果如表1，从试验结果可以看出 *GPS* 定位定向系统方位的测量精度为0.052度（*RMS*），优于1*mil*。表中受检点数值为精密多齿分度台示数，示值（平均值）为对应的 *GPS* 定位定向系统显示的数值。相邻差为相邻两次测量的误差（即为相邻两次测量结果之差减30度），累积误差为各次测量与第一次测量的误差。

表1 GPS定位定向系统方位角测试数据（单位：度）

受检点	示值（平均值）	相邻差	累积误差
0	33.71	-0.07	0
30	63.64	+0.05	-0.07
60	93.69	+0.09	-0.02
90	123.78	-0.05	+0.07
120	153.73	-0.02	+0.02
150	183.71	-0.08	0
180	213.63	+0.03	-0.08
210	243.66	+0.12	-0.05
240	273.78	-0.09	+0.07
270	303.69	-0.15	-0.02
300	333.84	+0.03	+0.13
330	3.87	+0.15	+0.16

参 考 文 献

1 Hatch R, Euler H J. Comparison of sever AROF kinematic technique. Proceeding of the 8th International Technical Meeting of the Satellite Division of the Institute of Navigation. Palm Springs, California: 1995, 363-370

2 胡国辉. 载波相位差分整周模糊度的求解. 南京大学学报（自然科学版）1997, 33: 163-165

3 Wei M, Lapucha D and Martell H. Fault detection and estimation in dynamic system, IAG symposia 107, 1990, 201-217